EXPRESS LETTER

Distinct rupture processes on a fault where M6-class earthquakes reoccurred in a short period: analysis of the 2011 and 2016 Northern Ibaraki, Japan, earthquakes using near-field waveforms

Kazuhito Hikima[1*]

Abstract

Crustal earthquakes are generally recognized as having recurrence periods of more than 1000 years. However, in northern Ibaraki Prefecture, Japan, two moderate-sized earthquakes occurred on almost the same fault plane in 2011 and 2016. Moreover, it has been reported that the slip distributions derived from crustal deformation data from these two events are almost identical. We performed a near-field waveform inversion analysis to estimate the details of the spatiotemporal distribution of the co-seismic rupture. Our results reveal large slip areas during each earthquake at different locations across the bend of the fault plane. These results indicate that the shear stress of the fault area where the main slip occurred during the 2011 event was not rebuilt in such a short period, a phenomenon that had not previously been discussed for this sequence. Our results also suggest that the fault geometry affected such complex fault ruptures.

Keywords Crustal earthquake, Earthquake recurrence, Rupture process, Near-field waveform, Bending fault
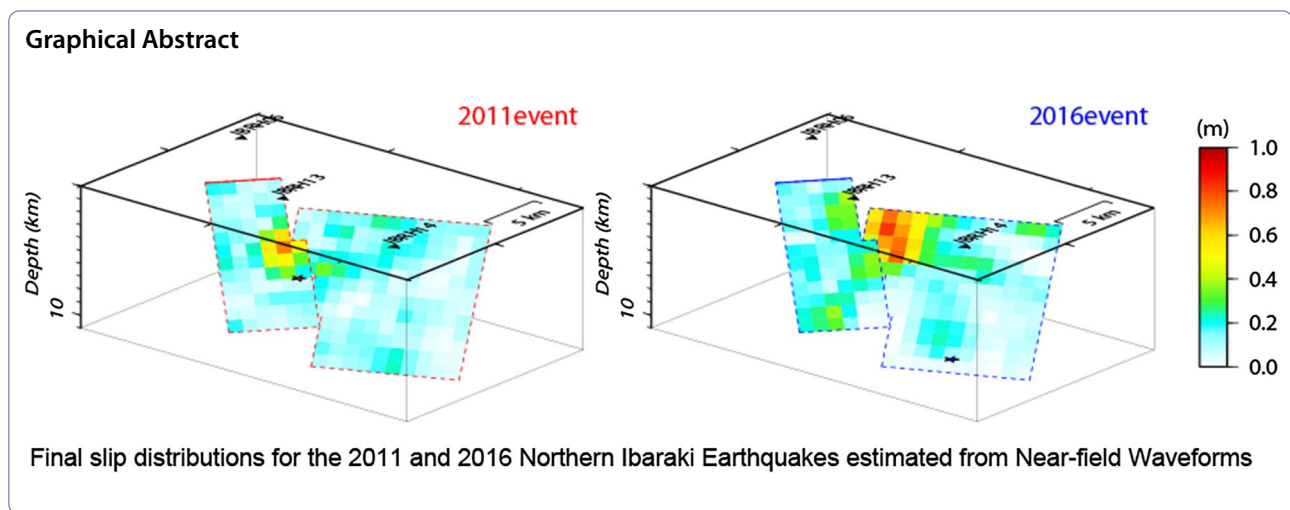
*Correspondence:
Kazuhito Hikima
hikima.kazuhito@tepco.co.jp
Full list of author information is available at the end of the article

Graphical Abstract

Final slip distributions for the 2011 and 2016 Northern Ibaraki Earthquakes estimated from Near-field Waveforms

Introduction

In northern Ibaraki Prefecture on the eastern coast of Honshu, Japan, facing the source area of the 11 March 2011 Tohoku-Oki earthquake (moment magnitude M_W 9.0), a moderate earthquake of M_J 6.3 (M_J refers to the magnitude scale determined by the Japan Meteorological Agency) occurred on 28 December 2016. However, in almost the same location, a comparable M_J 6.1 earthquake had previously occurred on 19 March 2011 (Fig. 1). The fault slip models of these earthquakes have almost identical fault planes and slip distributions, according to inversion analyses of the crustal deformation data (Fukushima et al. 2018; Kobayashi 2017). These prior results indicate that the fault plane slipped with an interval of only approximately 5.8 years. However, crustal earthquakes, which occur in Earth's upper crust, are recognized as typically having recurrence periods of 1000 years or more. Therefore, this singular phenomenon gives significant information on the occurrence of crustal earthquakes. However, the source analyses appear to have limited time resolution because they were performed using static deformation data.

According to Fukushima et al. (2018), the causes for the extremely early recurrence were (1) that exceptionally large post-seismic deformation following the first M_J 6.1 event rebuilt the shear stress on the fault and (2) that the rapid and sizeable post-seismic deformation of the 2011 Tohoku-Oki earthquake also promoted such afterslip. The afterslip of the first M_J 6.1 event is considerable, and it should be considered that source process analysis using interferometric synthetic aperture radar (InSAR), which was the main approach used in the analysis by Fukushima et al. (2018), may contain not only co-seismic slip but also post- and pre-seismic slip. This is because these InSAR images were obtained by taking the difference between the satellite images before and after the earthquake. Wimpenny et al. (2022) provided a more detailed discussion of the causes of the early recurrence, using not only crustal deformation data but also far-field seismic records. However, they did not present a new slip model but instead followed the slip distributions determined by Fukushima et al. (2018). Therefore, source process analysis with high-temporal-resolution data is also required to derive detailed co-seismic slip distributions for the 2011 and 2016 events. We should examine the causes of the recurrence of these events, considering co-seismic source models derived in this manner.

In this study, we performed a waveform inversion analysis using near-field strong ground motions to construct detailed spatiotemporal source models of these earthquakes, updating our previous results (Hikima 2017). Although some research groups have performed similar studies (Uchide et al. 2018; Tanaka and Iwakiri 2017), we performed the analysis assuming a bending fault geometry based on the detailed hypocenter distributions (Kato et al. 2017). In this paper, we first report the seismic moments for these events collected from catalog data and demonstrate that the results using InSAR data contain slips other than co-seismic slips, especially for the 2011 event. Then, we show the co-seismic slip results for both events and discuss the causes of the difference between the slip distributions using crustal deformations and our results. Finally, we discuss potential scenarios from the 2011 event to the 2016 event.

Moment release for each event

Earthquake parameters, including magnitude (seismic moment), are routinely determined and published by some institutions in publicly available databases. The magnitudes and seismic moments for the 2011 and
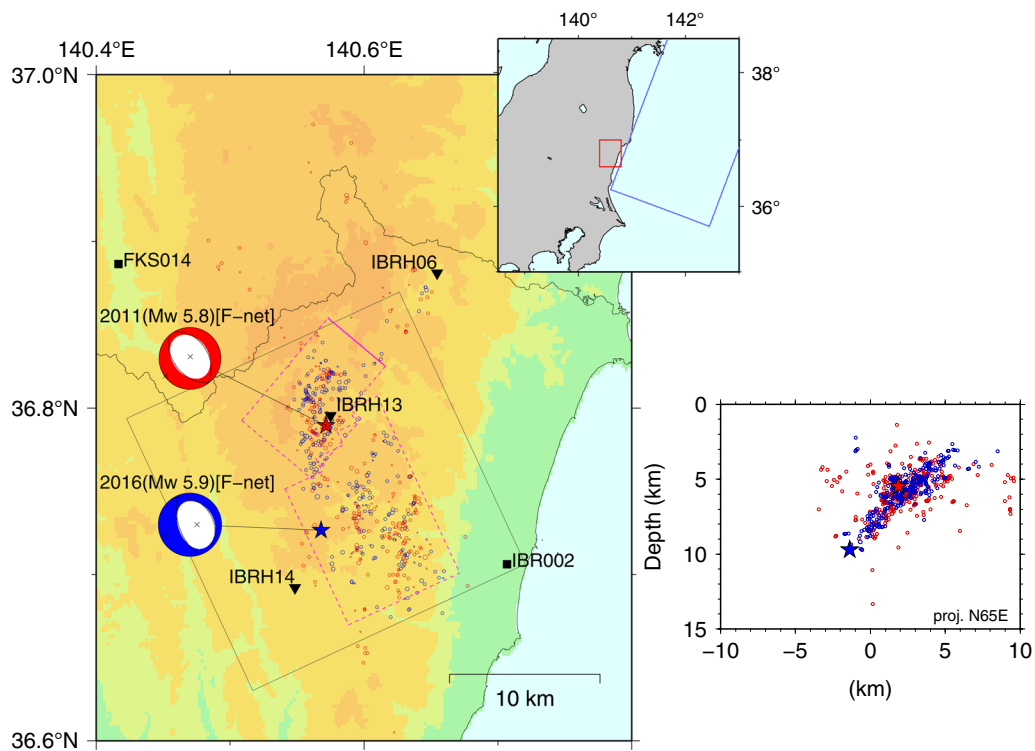
Fig. 1 Map of the target area of this study. The upper right inset shows the surrounding area of Honshu, Japan; the red frame indicates the area of the main map, and the blue area corresponds to the fault of the 2011 Tohoku-Oki earthquake. The red and blue stars in the main map represent the epicenters of the 2011 and 2016 events, respectively, and the centroid moment tensor (CMT) solutions by F-net are plotted using the corresponding colors. The strong motion stations used in the inversion analysis are shown as inverted triangles for KiK-net and squares for K-NET. The fault planes of the target events are depicted by purple dashed and solid lines. Aftershocks within 48 h of each event are plotted as red and blue dots for the 2011 and 2016 events, respectively (Kato et al. 2017). The right figure shows a depth cross-section of the hypocenters in the rectangular area bounded by a thin grey line on the main map

2016 northern Ibaraki earthquakes, taken from these databases, are listed in Table 1. Those reported by the JMA-CMT and F-net are determined by moment tensor analysis using the local seismic networks of Japan, and those by GCMT (Dziewonski et al. 1981; Ekström et al. 2012) are solutions using global network waveforms.

These moment magnitudes are consistent, and the M_W of the 2011 and 2016 events are 5.8 and 5.9, respectively. Notably, the 2011 event is smaller than the 2016 event. However, the moment magnitudes determined from InSAR data for the 2011 and 2016 events are 6.13 and 5.90, respectively (Fukushima et al. 2018). Therefore, the

Table 1 Moment magnitudes for the 2011 and 2016 events from different databases

Catalog	Moment magnitude M_w (seismic moment M_0)	
	2011 event	2016 event
JMA-CMT [*1]	M_w 5.8 ($M_0 = 7.5 \times 10^{17}$ Nm)	M_w 5.9 ($M_0 = 9.4 \times 10^{17}$ Nm)
F-net [*2]	M_w 5.8 ($M_0 = 6.35 \times 10^{17}$ Nm)	M_w 5.9 ($M_0 = 9.0 \times 10^{17}$ Nm)
GCMT [*3]	M_w 5.8 ($M_0 = 6.92 \times 10^{17}$ Nm)	M_w 5.9 ($M_0 = 7.92 \times 10^{17}$ Nm)
This study	M_w 5.8 ($M_0 = 7.0 \times 10^{17}$ Nm)	M_w 5.9 ($M_0 = 9.9 \times 10^{17}$ Nm)
Fukushima et al. (2018)	M_w 6.13 ($M_0 = 1.97 \times 10^{18}$ Nm)	M_w 5.90 ($M_0 = 8.91 \times 10^{17}$ Nm)

[*] 1) https://www.data.jma.go.jp/eqev/data/bulletin/eqdoc.html

[*] 2) https://www.fnet.bosai.go.jp/freesia/top.php?LANG=en

[*] 3) https://www.globalcmt.org/

seismic moment for the 2011 event is more than twice to that for the 2016 event, and the magnitude relationship between these events is opposite that for the co-seismic moment release estimated from the waveforms.

Because the magnitudes of the 2016 event are approximately the same for both the seismic and geodetic data, these results can be considered to correspond to co-seismic moment release. Conversely, it is thought that the estimation of the 2011 event using the InSAR data contains a significant amount of moment release from causes other than co-seismic slip. Although Fukushima et al. (2018) mention the possibility of the influence of an M_J 5.7 event occurring in the satellite image period, such a small event alone cannot explain the difference between the results obtained from the waveforms and the InSAR data. This is strong evidence that other causes, such as the afterslip of the 2011 Ibaraki event or the effect of the 2011 Tohoku-Oki earthquake, are included in the InSAR data results.

Consequently, it is necessary to estimate the detailed spatiotemporal co-seismic slip distributions for both events before discussing potential scenarios underlying the events. Source process inversion analysis using near-field waveforms is crucial for this purpose.

Rupture process inversion
Fault plane geometry
We first set the fault plane for estimating the rupture processes from the waveform data. Because fault planes are often configured using the hypocenter locations of the main shock and early aftershocks, these should be as accurate as possible. Around the northern Ibaraki area, dense seismic networks of approximately 60 portable stations equipped with short-period sensors were deployed to monitor the activated seismicity after the 2011 Tohoku-Oki earthquake (Kato et al. 2013). The hypocenters of the 2011 and 2016 Ibaraki events have also been determined using these data (Kato et al. 2017), and these parameters are suitable for considering the fault planes of these events.

In Additional file 1: Figure S1 (see the Additional file), the aftershocks determined by Kato et al. (2017), which occurred within 48 h after each mainshock of the 2011 and 2016 events, are plotted in different colors. The high degree of overlap between the aftershock distributions suggests that both events occurred on approximately identical fault planes (Kato et al. 2017). In the depth cross sections, strongly aligned dipping toward the southwest is clearly visible in the southern part of the aftershock area. In contrast, the alignment tends to be blurred in the northern portion near the hypocenter of the 2011 event. When these results are projected to other cross sections with a different strike angle, the aftershocks in the northern part align more clearly. Furthermore, it is difficult to place the hypocenters of the 2011 and 2016 main shocks on the same flat plane with the aftershocks. Therefore, the aftershock distributions suggest a curved fault surface, which is consistent with the results estimated using the geodetic data (Fukushima et al. 2018).

Considering these conditions, we configured the fault as two flat planes to approximate a curved surface, with a strike of 130° and dip of 42° for the northern plane and a strike of 155° and dip of 47° for the southern plane. The total length was 19 km, and the width was 12 km. These planes have been commonly used to estimate the slip distributions for the 2011 and 2016 events. In Figs. 1 and Additional file 1: Fig. S1, these fault planes are projected onto the ground surface, and the aftershocks of each event are also plotted. The hypocenters of the 2011 and 2016 events (Kato et al. 2017) are on the northern and southern planes, respectively. Furthermore, the northern plane was shifted to a shallower depth so that its top reached the ground surface, to account for the surface deformation found in the northern area (Fukushima et al. 2018; Komura et al. 2019).

Methods and data
The rupture process inversion analysis was performed using multiple time-window methods (Yoshida et al. 1996; Hikima and Koketsu 2005). The fault models were divided into 1 km × 1 km subfaults, and the slip histories were represented by a combination of ramp functions with a rise time of 0.5 s. The slip vectors were represented by a linear combination of two components in the directions of −90° ± 45° considering normal faults obtained by the centroid moment tensor (CMT) solutions.

We used acceleration waveforms recorded at 16 stations (Additional file 1: Figure S2) selected from the K-NET and KiK-net strong ground motion networks (Aoi et al. 2004; NIED 2019) for their close proximity to the source area and their records of both the 2011 and 2016 events. We expected that using an identical set of stations for each event would increase the reliability of the relative slip distribution between the two events. Furthermore, records from the IBRH13 station, located just above the source fault (Fig. 1), also contribute to providing detailed slip distributions. The three-component accelerograms were numerically integrated to obtain velocity waveforms, which were filtered with a pass band of 0.05–0.8 Hz and re-sampled with a 0.2-s sampling rate.

Because Green's functions (theoretical waveforms) are calculated using the reflectivity method (Kohketsu 1985), they require one-dimensional stratified velocity models. To obtain accurate Green's functions, we applied an inverse technique (Hikima and Koketsu 2005; Ichinose et al. 2003) to tune velocity models adapted to

each station. To this end, we used the seismograms from the moderate magnitude event within the source area (19 February 2012, M_W 4.9). The initial models for each station were obtained as the vertical profile at the objective position in the three-dimensional velocity model (Koketsu et al. 2012). The resultant velocity models are shown in Additional file 1: Figure S3.

Results

The estimated final slip distributions for the 2011 and 2016 events are shown in Fig. 2. The waveforms calculated using these slips show good agreement with the observed waveforms (Additional file 1: Figure S4). This indicates that these results are appropriate for these events. The seismic moment and the maximum slip for the 2011 event are $M_0 = 7.5 \times 10^{17}$ Nm (M_W 5.8) and 0.7 m, respectively, and those for the 2016 event are $M_0 = 9.9 \times 10^{17}$ Nm (M_W 5.9) and 0.8 m, respectively. The moment magnitudes are almost equal to the CMT values estimated from seismic waveforms (Table 1). However, the inverted moment release for the 2011 event is lower than the estimation from the InSAR data (Fukushima et al. 2018). As mentioned previously, the result for the 2011 event estimated using waveforms is thought to correspond to only co-seismic slip, whereas the estimate based on the InSAR data includes considerable afterslip.

Focusing on each slip distribution, the large slip area (asperity) of the 2011 event is located on the northern part of two fault planes, whereas the asperity of the 2016 event is on the southern part. To clearly display
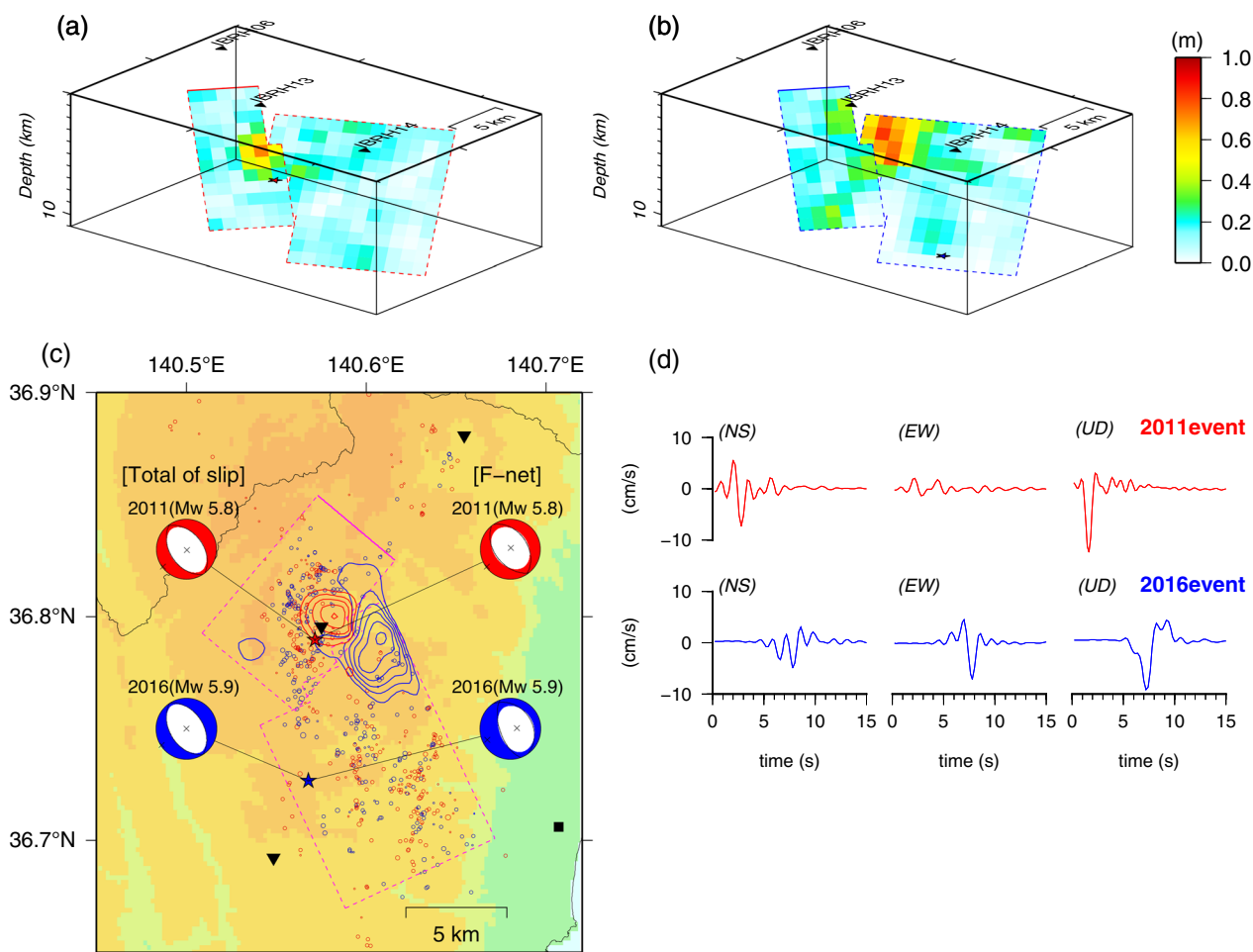

Fig. 2 Estimated final slip distributions for each event. These are bird's-eye views from the southwest for the **a** 2011 and **b** 2016 events. **c** Distribution of slips greater than 0.3 m for the two events projected onto the horizontal plane and superimposed at 0.1 m intervals. Aftershocks that occurred within 48 h of each event (Kato et al. 2017) are also plotted. The total moment tensors for each event and the CMT solution obtained by F-net are displayed for comparison. The 2011 and 2016 events are shown in red and blue, respectively. The black inverted triangles and squares denote observation stations, as in Fig. 1. **d** Velocity waveforms at the IBRH13 station. Upper red traces depict the 2011 event, and lower blue traces show those for the 2016 event. Every trace is plotted from the origin time for each event
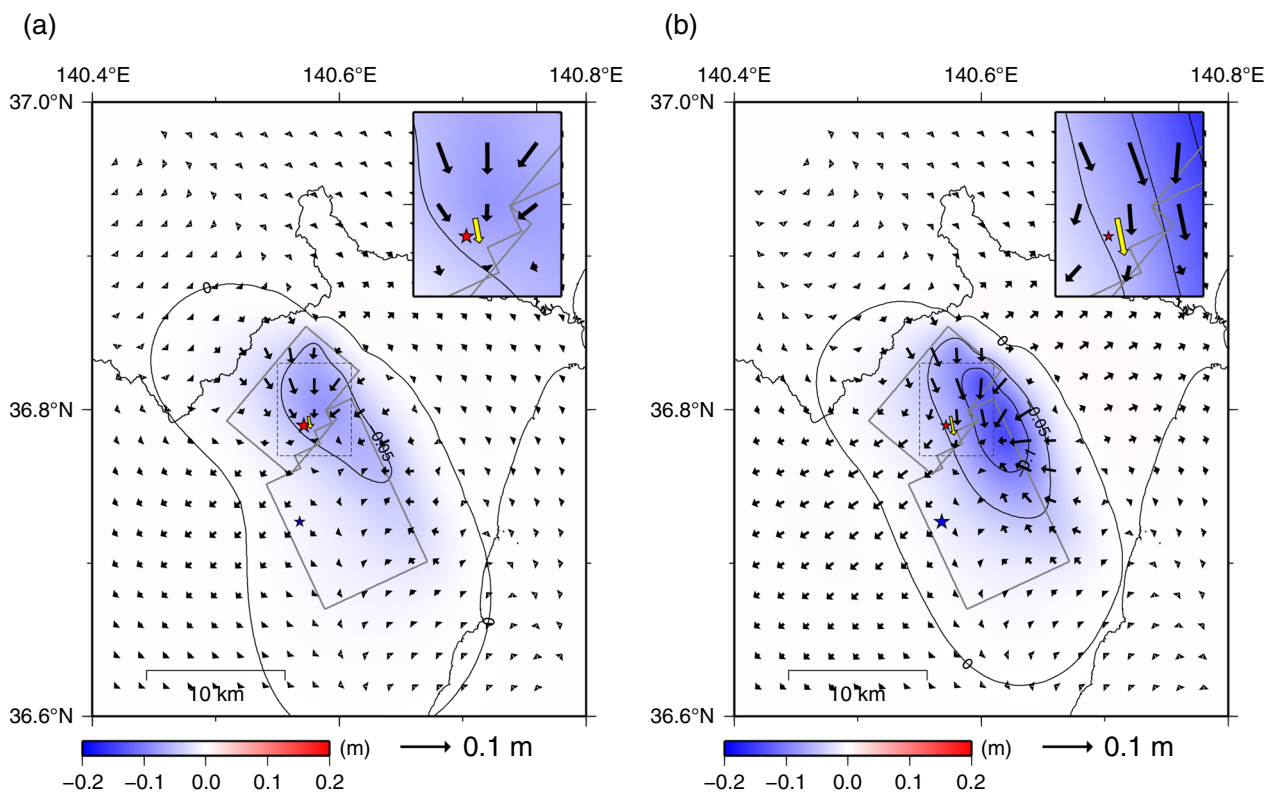
Fig. 3 Calculated surface deformations assuming the derived slip distributions for the **a** 2011 and **b** 2016 events. The vector field represents the horizontal deformation, and the color contour shows the vertical deformation. Yellow arrows correspond to the observed permanent displacement at IBRH13 (see Additional file 1: Figure S6). The insets show enlarged maps of the areas indicated by the dashed lines in the main figures. Note that the vectors in the insets are magnified by a factor of two relative to those in the main figure

the interrelationships, slip distributions greater than 0.3 m are projected onto the ground surface and superimposed with the aftershocks of each event in Fig. 2c. This reveals that the asperities have little mutual overlap, and those that do are located adjacent to each other across the bending part. Furthermore, there are few aftershocks on and around the asperities, as often seen in the relations between large slip areas and aftershocks (e.g., Mendoza and Hartzell 1998; Das and Henry 2003). In addition, it can also be seen that the number of aftershocks associated with the 2011 event is low around the asperity for the 2016 event (see also Additional file 1: Figure S5 for cross-sectional plots).

These results demonstrate that the 2011 event caused little slip at the location of the asperity for the 2016 event. Additionally, it may be possible to conclude that the coupling part, which became the asperity for the 2016 event, had already existed during the 2011 event from the perspective of the co-seismic slip distributions and aftershock patterns. Therefore, the co-seismic slip distribution derived using the waveforms suggests that the main part of the 2016 event is the "slip residue" of the 2011 event.

Discussion

Validation of results and differences from results obtained from InSAR data

The slip distributions obtained from the waveforms differ in detail from those obtained from the InSAR data. Therefore, the inversion analysis and resultant slip distributions should be verified before discussing the process underlying the recurrence. Furthermore, it is necessary to consider the cause of the different slip distributions obtained from the waveforms and the InSAR data.

To confirm the complementary asperity distributions for the 2011 and 2016 events, we compared the waveforms for these events directly. The waveforms for the two events at the IBRH13 station, which is located just above the fault surface (Fig. 1), are shown in Fig. 2d. The waveforms recorded at this station during the two events have different characteristics. Specifically, the maximum amplitude of the north–south (NS) component is larger than that for the east–west (EW) component for the 2011 event, whereas the opposite is true for the 2016 event. This means that the arrival directions from the main slips are different if the fault mechanisms are almost the same. This is consistent with the

waveform inversion results, which indicate that the co-seismic asperities follow different directions from IBRH13.

Next, we discuss the disparity of the seismic moments in the results obtained from the waveforms and the InSAR data. We calculated surface deformations assuming the slip distributions obtained by waveform inversions (Fig. 3). These deformations were calculated assuming a homogeneous half-space (Okada 1992). The calculated patterns are similar to the observed InSAR images (Fukushima et al. 2018). However, the average deformation for the 2011 event is smaller than that for the 2016 event in the calculated distributions, whereas the opposite is true in the observed InSAR data. To compare these results with the actual co-seismic deformations, we estimated the permanent displacements by taking the double integral of the accelerograms at the IBRH13 station (Additional file 1: Figure S6). The derived co-seismic displacement for the 2011 event, which is 2.5 cm to the south, 0.45 cm to the east, and 8.6 cm downward, is smaller than that for the 2016 event, which is 3.8 cm to the south, 0.74 cm to the east, and 6.7 cm downward. These displacements are almost consistent with that calculated from the derived co-seismic fault slip distributions (Fig. 3). From this discussion, the slip distribution obtained in this study is reasonable for co-seismic slip, whereas the 2011 slip distribution determined from

the InSAR data also includes a considerable amount of early afterslips immediately following the main shock.

Although the slip distribution estimated from the InSAR data includes the effect of afterslip, it is true that the main slip for the 2016 event overlaps with the slip distribution near the time of the 2011 event. However, when the afterslip is equal to or larger than the main shock that occurred at the time of the 2011 event, it is possible that the geodetic data may not be detected due to insufficient resolution, even if part of the fault plane remains locked. Therefore, based on the co-seismic slip distribution for the 2011 event, we made a hypothetical model in which the total seismic moment was more than doubled without changing the slips at the asperities for the 2011 and 2016 events and calculated the surface deformation (Additional file 1: Figure S7). The results confirm that the synthetic crustal deformation was similar to the pattern for the 2011 event, and the distinct deformation pattern associated with the slip deficit at the asperity for the 2016 event was not recognized. Namely, the possibility that the portion that would be the asperity for the 2016 event had remained locked even after the 2011 event is not ruled out by the InSAR data.

Rupture scenario from the 2011 event to the 2016 event

The rupture histories for each event are shown in Fig. 4 to elucidate the co-seismic slip for these events and to
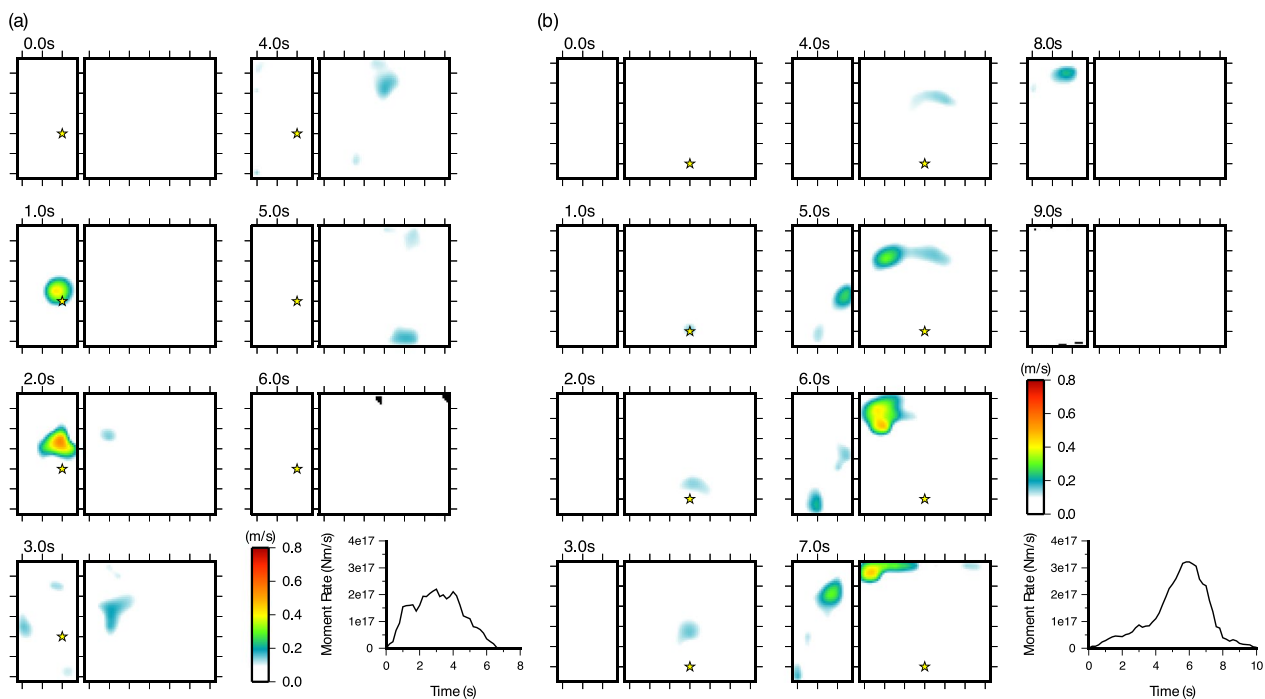

Fig. 4 Snapshots of the slip velocity at intervals of 1 s derived by source process inversions for the **a** 2011 and **b** 2016 events. The yellow star denotes the hypocenters of each event. The moment rate functions are also shown

discuss corresponding scenarios for the 2011 to 2016 events. The plots in Fig. 4 show snapshots of the slip velocity in intervals of 1 s. These snapshots show that the two events have somewhat different time histories. Namely, the 2011 event slipped primarily near its hypocenter with a relatively high speed. In contrast, during the 2016 event, the rupture began at the southern hypocenter, propagated slowly toward the north, and finally ruptured the asperity, located at the northern edge of the southern fault. Therefore, in simple terms, the 2011 event ruptured more rapidly than did the 2016 event.

Considering these slip histories, we hypothesize that the relationship between the 2011 and 2016 events is as follows. The 2011 event occurred as an ordinary earthquake and slipped largely near the hypocenter. However, the adjacent area across the bend did not slip at that time. After that, the area remained locked until the 2016 event. At the time of the 2016 event, the rupture started at a distance from its asperity, and rupture propagation or seismic waves excited the locked area, which thus became a large slip area. The propagation speed appeared to be slow because the asperity slipped as if induced. It may be possible that the large afterslip for the 2011 event and the 2011 Tohoku-Oki earthquake caused stress to accumulate around the source area, as suggested by the crustal deformation analysis (Fukushima et al. 2018), although it is not the same area as the 2011 event.

Finally, we would like to consider why the asperity for the 2016 earthquake did not rupture during the 2011 event. Of course, it is possible that the stress accumulation at the asperity for the 2016 event was insufficient for slip to occur at the time of the 2011 event. In addition, it is possible that the fault geometry—specifically, the bending between the asperities—contributed to the co-seismic slip. Additional file 1: Figure S8 shows the Coulomb failure stress (ΔCFF) calculated for the southern fault, assuming the slip distribution on the northern fault for the 2011 event. A negative value is calculated at the northern edge of the southern fault, and it shows that the slip was suppressed near the southern area of the bending zone. Although this calculation is simplified and contains many uncertainties, the bending of a fault tends to inhibit rupture (e.g., Kame and Yamashita 1999, 2003; Biasi and Wesnousky 2017). On the other hand, at the time of the 2016 event, the asperity was likely easily ruptured because the hypocenter and the asperity were on the same plane.

Because of the bending of the fault, this sequence of seismic activity—namely, halting of the initial rupture being followed by a rupture from another hypocenter in the place where large slip did not initially occur—has been observed in the past, e.g., in the 2003 northern Miyagi earthquakes (Hikima and Koketsu 2004). Earlier reported examples have also shown that changes in stress caused by earlier earthquakes induce moderate-scale earthquakes (e.g., Hikima and Koketsu 2005). Therefore, the 2011 and 2016 events in northern Ibaraki Prefecture can be considered to be cases where fault geometry plays a role in recurrence, although the interval is not so short (approximately 5.8 years).

Conclusion

We performed a near-field waveform inversion analysis to derive a detailed spatiotemporal rupture history of the 2011 and 2016 northern Ibaragi prefecture earthquakes. Large slip areas during each earthquake were obtained at different locations across the bend of the fault plane. These earthquakes can be viewed as a series of ruptures on the same fault plane rather than simply due to the rebuilding of shear stress at the same location.

Supplementary Information

The online version contains supplementary material available at https://doi.org/10.1186/s40623-023-01928-y.

Additional file 1: Additional figures S1–S8.

Availability of data and materials

The K-NET and KiK-net waveforms used for rupture process inversion analyses in the study are available at the NIED server webpage (https://www.kyoshin.bosai.go.jp/kyoshin/search/index_en.html) or DOI link (https://www.doi.org/10.17598/NIED.0004) with free registration. The CMT solutions listed in Table 1 for JMA-CMT, F-net, and GCMT are available on their respective webpages (https://www.data.jma.go.jp/eqev/data/bulletin/eqdoc.html, https://www.fnet.bosai.go.jp/freesia/top.php?LANG=en, https://www.globalcmt.org/). The Generic Mapping Tools (GMT) software (Wessel & Smith 1998) was used in this study.

Declarations

Competing interests

The author declares that they have no competing interests.

Author details
[1]Tokyo Electric Power Company Holdings, Inc., TEPCO Research Institute, Yokohama, Japan.

References

Aoi S, Kunugi T, Fujiwara H (2004) Strong-motion seismograph network operated by NIED: K-NET and KiK-net. J Jpn Assoc Earthquake Eng. https://doi.org/10.5610/jaee.4.3_65

Biasi GP, Wesnousky SG (2017) Bends and ends of surface ruptures. Bull Seismol Soc Am 107(6):2543–2560. https://doi.org/10.1785/0120160292

Das S, Henry C (2003) Spatial relation between main earthquake slip and its aftershock distribution. Rev Geophys 41:3. https://doi.org/10.1029/2002RG000119

Dziewonski AM, Chou A, Woodhouse JH (1981) Determination of earthquake source parameters from waveform data for studies of global and regional seismicity. J Geophys Res Solid Earth 86(B4):2825–2852. https://doi.org/10.1029/JB086iB04p02825

Ekström G, Nettles M, Dziewoński AM (2012) The global CMT project 2004–2010: Centroid-moment tensors for 13,017 earthquakes. Phys Earth Planet Inter 200–201:1–9. https://doi.org/10.1016/j.pepi.2012.04.002

Fukushima Y, Toda S, Miura S, Ishimura D, Fukuda J, Demachi T, Tachibana K (2018) Extremely early recurrence of intraplate fault rupture following the Tohoku-Oki earthquake. Nat Geosci 11:777–781. https://doi.org/10.1038/s41561-018-0201-x

Hikima, K. (2017) Source processes of the M 6 class earthquakes which occurred in northern Ibaraki Prefecture on 2011 and 2016. Paper presented at JpGU-AGU Joint Meeting 2017, Makuhari, Japan, SSS15-01. https://confit.atlas.jp/guide/event/jpguagu2017/subject/SSS15-01/advanced

Hikima K, Koketsu K (2004) Source processes of the foreshock, mainshock and largest aftershock in the 2003 Miyagi-ken Hokubu, Japan, earthquake sequence. Earth Planet Space 56:87–93. https://doi.org/10.1186/BF03353392

Hikima H, Koketsu K (2005) Rupture processes of the 2004 Chuetsu (mid-Niigata prefecture) earthquake, Japan: a series of events in a complex fault system. Geophys Res Lett 32:L18303. https://doi.org/10.1029/2005GL023588

Ichinose GA, Thio HK, Somerville PG, Sato T, Ishii T (2003) Rupture process of the 1944 Tonankai earthquake (Ms 8.1) from the inversion of teleseismic and regional seismograms. J Geophys Res Solid Earth. https://doi.org/10.1029/2003JB002393

Kame N, Yamashita T (1999) A new light on arresting mechanism of dynamic earthquake faulting. Geophys Res Lett 26(13):1997–2000. https://doi.org/10.1029/1999GL900410

Kame N, Yamashita T (2003) Dynamic branching, arresting of rupture and the seismic wave radiation in self-chosen crack path modeling. Geophys J Int 155(3):1042–1050. https://doi.org/10.1111/j.1365-246X.2003.02113.x

Kato A, Igarashi T, Obara K, Sakai S, Takeda T, Saiga A et al (2013) Imaging the source regions of normal faulting sequences induced by the 2011 M9.0 Tohoku-Oki earthquake. Geophys Res Lett 40:273–278. https://doi.org/10.1002/grl.50104

Kato, A., Sakai, S., Iidaka, T., Obara, K. (2017) Very short recurrence interval of M~6 earthquakes within the common fault zone. Paper presented at JpGU-AGU Joint Meaeting 2017, Makuhari, Japan, SCG62-P03. https://confit.atlas.jp/guide/event/jpguagu2017/subject/SCG62-P03/advanced

Kobayashi, T. (2017) Normal-faulting earthquakes in the northern area of Ibaraki Prefecture, Japan in 2011 and 2016 - Duplicate events detected by InSAR observations. Paper presented at IAG-IASPEI 39th Joint Scientific Assembly, Kobe, Japan, J09-1-01. http://www.iaspei.org/assemblies-conferences/2017-iag-iaspei-39th-joint-scientific-assembly-kobe-japan

Kohketsu K (1985) The extended reflectivity method for synthetic nearfield seismograms. J Phys Earth 33:121–131. https://doi.org/10.4294/jpe1952.33.121

Koketsu K, Miyake H, Suzuki H (2012) Japan Integrated Velocity Structure Model Version 1. Paper presented at 15th World Conference on Earthquake Engineering 2012, Lisbon, Portugal

Komura K, Aiyama K, Nagata T, Sato HP, Yamada A, Aoyagi Y (2019) Surface rupture and characteristics of a fault associated with the 2011 and 2016 earthquakes in the southern Abukuma Mountains, northeastern Japan, triggered by the Tohoku-Oki earthquake. Earth, Planets and Space 71(1):1–23. https://doi.org/10.1186/s40623-019-1085-8

Mendoza C, Hartzell S (1998) Aftershock patterns and main shock faulting. Bull Seismol Soc Am 78(4):1438–1449. https://doi.org/10.1785/BSSA0780041438

NIED (2019) NIED K-NET, KiK-net, National Research Institute for Earth Science and Disaster Resilience. https://doi.org/10.17598/NIED.0004

Okada Y (1992) Internal deformation due to shear and tensile faults in a half-space. Bull Seismol Soc Am 82(2):1018–1040. https://doi.org/10.1785/BSSA0820021018

Tanaka M, Iwakiri K (2017) Source processes of the two Ibaraki earthquakes and comparison between their rupture areas. Paper presented at the Seismological Society of Japan 2017 Fall Meeting, Kagoshima, Japan.

Uchide T, Ohtani M, Takahashi M, Imanishi K (2018) Rupture processes and geophysical background of the 2011 and 2016 Northern Ibaraki Prefecture earthquakes. Paper presented at the 12th Joint Meeting of the UJNR Panel on Earthquake Research, Kumamoto, Japan, O-34. https://cais.gsi.go.jp/UJNR/12th/document/abst/O-34.pdf

Wessel P, Smith WHF (1998) New, improved version of generic mapping tools released. Eos Trans AGU 79(47):579

Wimpenny S, Forrest N, Copley A (2022) Time-dependent decrease in fault strength in the 2011–2016 Ibaraki-Fukushima earthquake sequence. Geophys J Int 232(2):788–809. https://doi.org/10.1093/gji/ggac368

Yoshida S, Koketsu K, Shibazaki B, Sagiya T, Kato T, Yoshida Y (1996) Joint inversion of near- and far- field waveforms and geodetic data for the rupture process of the 1995 Kobe earthquake. J Phys Earth 44:437–454. https://doi.org/10.4294/jpe1952.44.437

Publisher's Note